Available online at www.sciencedirect.com
SCIENCE DIRECT®
Journal of Volcanology and Geothermal Research 152 (2006) 157–173
Journal of volcanology and geothermal research
www.elsevier.com/locate/jvolgeores

# Ground deformation at Soufrière Hills Volcano, Montserrat during 1998–2000 measured by radar interferometry and GPS

G. Wadge [a,*], G.S. Mattioli [b], R.A. Herd [c,1]

[a] *Environmental Systems Science Centre, University of Reading, UK*
[b] *Department of Geosciences, University of Arkansas, USA*
[c] *Montserrat Volcano Observatory, Montserrat, West Indies*

Received 11 January 2005; received in revised form 9 September 2005; accepted 3 November 2005
Available online 4 January 2006

**Abstract**

We examine the motion of the ground surface on the Soufrière Hills Volcano, Montserrat between 1998 and 2000 using radar interferometry (InSAR). To minimise the effects of variable atmospheric water vapour on the InSAR measurements we use independently-derived measurements of the radar path delay from six continuous GPS receivers. The surfaces providing a measurable interferometric signal are those on pyroclastic flow deposits, mainly emplaced in 1997. Three types of surface motion can be discriminated. Firstly, the surfaces of thick, valley-filling deposits subsided at rates of 150–120 mm/year in the year after emplacement to 50–30 mm/year two years later. This must be due to contraction and settling effects during cooling. The second type is the near-field motion localised within about one kilometre of the dome. Both subsidence and uplift events are seen and though the former could be due to surface gravitational effects, the latter may reflect shallow (<1 km) pressurisation effects within the conduit/dome. Far-field motions of the surface away from the deeply buried valleys are interpreted as crustal strains. Because the flux of magma to the surface stopped from March 1998 to November 1999 and then resumed from November 1999 through 2000, we use InSAR data from these two periods to test the crustal strain behaviour of three models of magma supply: open, depleting and unbalanced. The InSAR observations of strain gradients of 75–80 mm/year/km uplift during the period of quiescence on the western side of the volcano are consistent with an unbalanced model in which magma supply into a crustal magma chamber continues during quiescence, raising chamber pressure that is then released upon resumption of effusion. GPS motion vectors agree qualitatively with the InSAR displacements but are of smaller magnitude. The discrepancy may be due to inaccurate compensation for atmospheric delays in the InSAR data.


*Keywords:* ground deformation; radar interferometry; GPS; magma supply

## 1. Introduction

The 1995–present eruption of Soufrière Hills Volcano on Montserrat has been, in many respects, an ordinary example of a Peléean dome eruption (Druitt and Kokelaar, 2002). But in one respect it has been extraordinary: the magma flux through the volcano and onto the surface increased systematically during the first two to three years (Sparks et al., 1998) then declined to zero (Norton et al., 2002), and 20 months later surface effusion of lava resumed in a second phase of sustained dome growth. Long-lived andesitic eruptions like this one do provide a valuable natural experiment to test ideas about how

* Corresponding author. Tel.: +44 118 3786412; fax: +44 118 3786413.
*E-mail address:* gw@mail.nerc-essc.ac.uk (G. Wadge).
[1] Currently University of Hawaii, USA.

0377-0273/$ - see front matter © 2005 Elsevier B.V. All rights reserved.
doi:10.1016/j.jvolgeores.2005.11.007

magma is supplied and stored beneath subduction zone volcanoes. In the case of Soufrière Hills Volcano the main observed variable of this is that the magma flux accelerated from November 1995 to March 1998, stopped until November 1999 (a period of no lava effusion), and then resumed at near constant rates (a period of lava effusion) (Herd et al., 2004). How can that pattern be explained? Of particular interest here is the role played by a crustal magma reservoir in the buffering of deep magma supply and extrusion to the surface. We might expect that any such buffering role would involve elastic deformation of the brittle crust above the volcano (e.g., Dvorak and Dzurisin, 1997) and that this would find expression as motion of the surface. Thus measurements of surface deformation across the hiatus may allow us to examine this in detail.

Soufrière Hills Volcano is a far from ideal setting in which to make surface deformation measurements. Measurement stations and instruments can and have been destroyed by pyroclastic flows and ground access requires special efforts. Despite this, Electronic Distance Meter (EDM) measurements (Jackson et al., 1998) and GPS measurements (Mattioli et al., 1998, 2000, 2002a,b; Shepherd et al., 1998; Norton et al., 2002) have been made at various sites on and around the volcano since 1995. The lowermost flanks of the volcano are beneath the sea and measurements only out to 3–5 km from the central conduit are possible for all sectors except to the north (to 12 km). This means that for any source of stress 2 km or more below sea level a substantial portion of the surface strain field will be inaccessible. Nevertheless, even a partial mapping of the surface displacement field can give useful constraints to simple questions such as: Is the volcano inflating or deflating?

In this paper we present data from two geodetic techniques that use satellite technology: radar interferometry (InSAR) and Global Positioning System (GPS) from the three years, 1998–2000, that span the hiatus in magma supply. We test three hypothetical systems of supply using these data: an open system, an unbalanced system and a depleting system (Table 1). The use of InSAR data to measure surface displacement on basaltic volcanoes is well known (Amelung et al., 2000), but less so on andesitic stratovolcanoes (Pritchard and Simons, 2004) and very unusual during long-term eruption. The technique is prone to high levels of uncertainty under these conditions. We reduce the uncertainty of the measurement accuracy due to variable water vapour contents in the atmosphere (a common problem in InSAR and particularly at Montserrat) by correcting each interferogram with an explicit water vapour path difference field derived from continuous GPS receivers.

## 2. InSAR measurements

Repeat-pass, radar interferometry measurements of the Soufrière Hills Volcano have been made from satellites using the ERS-1 and -2, Radarsat and JERS-1 radars (Wadge et al., 2002a). In this study we use only the ERS data from 1998 to the end of 2000 in differential mode to measure the ground motion. Earlier studies of ERS data from Montserrat (Wadge et al., 1999, 2002a) have shown that:

1. Prior to the destruction of the forest and agricultural cover from 1995 to the present there were no suitable surfaces to measure long-term motion using the C-band SAR of ERS.
2. The surfaces of the pyroclastic flow deposits that provide most of the coherent phase signals generally show a gradual loss of that signal over periods of about one year. The sector of the volcano most prone to pyroclastic flows, the Tar River valley on the eastern slopes, decorrelates after a few weeks to months.
3. The lava dome at the summit of the volcano can decorrelate over much of its surface during periods of less than one day because of rockfall disturbances and thermally induced motions.

Table 1
Hypothetical magma supply systems for Soufrière Hills Volcano and the predicted deformation behaviour for 1998–2000

| Hypothetical system | Reservoir Behaviour | Deformation 1998–2000 | |
|---|---|---|---|
| Open | Balanced inflow and outflow of magma with no pressure variation | | None |
| Unbalanced | Outflow > inflow during lava effusion | 1997–March 98: | Subsidence |
| | Inflow during non-effusion | April 98–Nov 99 [no lava effusion]: | Uplift |
| | | Dec 99–Dec 00 [lava effusion]: | Subsidence |
| Depleting | No inflow | 1997–March 98: | Subsidence |
| | | April 98–Nov99 [no lava effusion]: | None |
| | | Dec 99–Dec 00 [lava effusion]: | Subsidence |

Thus we are restricted to specific areas of the volcano, and to temporal windows of no greater than about one year, over which to measure surface strain accumulation via ERS InSAR. One L-band JERS-1 interferogram (2 September 1996–24 May 1997) has more widespread area of coherence over vegetated terrain than the equivalent duration C-band ERS interferograms, but falls outside the period of this study. Between July 1997 and December 2000, 57 ERS SAR images were collected at intervals of 35 days (mainly) and 1 day. They were all from ascending passes of the ERS-1 and-2 satellites with the radar pointing almost to the east. Data from equivalent descending passes were not collected by the regional ground receiving station, though they were collected experimentally on Montserrat during 2000 (Wadge et al., 2000). Fortunately, Montserrat was in a region of overlap between neighbouring ascending image swaths and so there are two separate series of ascending images (tracks 075 and 347) with viewing angles a few degrees apart.

### 2.1. Data processing

The raw SAR data were focused to complex images and their orbital locations refined using ESA's precise orbit PRC data. After correction for the ellipsoid, the phase effects of topography were removed using a digital elevation model (DEM). This DEM was created from the pre-eruption topography and a photogrammetric model generated from stereo aerial photography flown on 8 February 1999 (Wadge, 2000). We consider it representative of the surface of the volcano during 1998–2000, except for the areas of the dome itself and the Tar River valley (Fig. 1) which were subject to pyroclastic flows and collapse events during this period. The root mean square vertical error of the DEM was estimated at about 10 m overall and about half this on the flatter surfaces, whence most of the InSAR signal derives. After applying an adaptive filter to reduce noise (Goldstein and Werner, 1998), the interferograms were unwrapped (removing any modulo 2 $\pi$ ambiguities) using a modified form of the Goldstein branch-cut algorithm (Ghiglia and Pritt, 1998). The unwrapping process between unconnected regions of the interferogram is independent and afterwards requires some assumptions and corrections to be made about possible offsets between the regions. This is usually straightforward. Because of the small size of Montserrat (10–16 km) we were not able to assess and correct for the effect of any residual orbital positioning errors, though these are likely to be small anyway over such short distances.

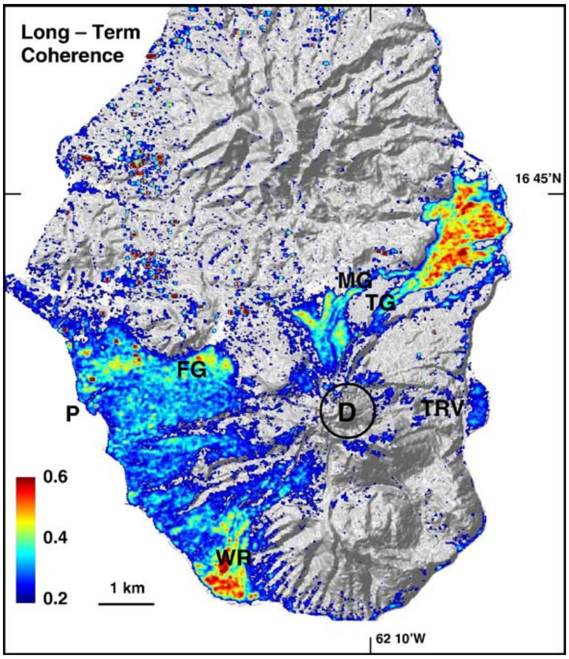


Fig. 1. Map of the long-term (1998–2000) coherence measured from ERS SAR phase returns from the surface of Montserrat. Note the low coherence on the lava dome of Soufrière Hills Volcano (D) and in the Tar River Valley (TRV). P marks the waterfront of the destroyed town of Plymouth, WR = White River, FG = Fort Ghaut, MG = Mosquito Ghaut and TG = Tuitt's Ghaut. Grey tone shows topography in areas of low coherence.

### 2.2. Data quality

Images of local spatial phase correlation, or coherence, were generated and summed to give an aggregate image of those surfaces that retained long-term coherence, an effective signal-to-noise measure for InSAR (Fig. 1). This value varies from zero, indicating no long-term coherence, to unity indicating complete coherence. The areas of major pyroclastic flow deposits to the northeast, southwest and west of the volcano show levels of coherence (>0.25) that yield quantitative differential results, but the dome and Tar River valley do not (Fig. 1). This loss of coherence with time is due to modification of the local scattering properties of the surface by erosion, deposition of new deposits and re-deposition of existing deposits. Also evident to the northwest of the volcano as points of very high coherence are the signals from a number of permanent scatterers (Fig. 1; Cabey and Wadge, 2001).

Although there are ERS SAR images of Montserrat from before the eruption began in 1995, there are no useable interferograms derived from these data because of a lack of unvegetated surfaces. Acquisition of ERS SAR data during the eruption began in mid-1997, but useful differential interferograms could only be constructed beginning in 1998. Not all of the images are suitable for interferometric processing. Sometimes the positions of the satellites at the times of acquisition of the two images needed to construct the interferogram were too far apart, the ideal for repeat-pass differential InSAR being identical viewing positions, giving a perpendicular baseline of 0 m. Also the ERS-2 satellite suffered from a degradation of pointing control during 2000 which meant an additional loss of useful data (Wadge et al., 2000). Fig. 2 shows what useful interferograms were obtained from the ERS SAR data after applying a quality control threshold of less than 350 m for the perpendicular baseline. This threshold, when coupled with the DEM, means that any residual topographic errors should contribute less than about 1 cm to the motion detection error, and about half this figure in the flatter areas. Note the sparsity of the data set for 1998.

Having considered the noise effects of radar geometry and the properties of the local surface we now turn to the third major source of noise, atmospheric path effects. For such a small area we can ignore any of the very long wavelength effects due to ionospheric variability. However, the effects due to variable water vapour contents in the troposphere are potentially significant (Hanssen, 2001). Higher water vapour content changes the refractive index of the atmosphere such that the passage of the radio wave is "delayed". For an interferometric pair, if the second image has higher water vapour content in one area relative to that in the first image then that area appears to be farther away and to have subsided with time relative to an area where the water vapour content has changed less. In such cases, techniques to help minimize the effects are necessary to derive geophysically meaningful results (Williams et al., 1998).

## 3. GPS-based water vapour correction of InSAR measurements

The GPS technique complements InSAR, as both employ microwave radiation that are affected in the same way by water vapour. GPS makes use of multiple path measurements through the troposphere to different satellites, and knowledge of the geometry of these paths means that the resultant variable delay effects can be used to model a total delay due to water vapour, usually mapped to the zenith, the Zenith Wet Delay (ZWD) (e.g., Bevis et al., 1992). On Montserrat, GPS receivers have been operating in continuous mode at up to six sites during the eruption (Mattioli et al., 2000, 2002a,b; Norton et al., 2002). The ZWD estimates from these GPS sites, at the times of ERS satellite overpasses, can be used to correct for the InSAR water vapour field delays. As Table 2 shows, there is a range of over 200 mm of path delay apparent from the ZWD data at the

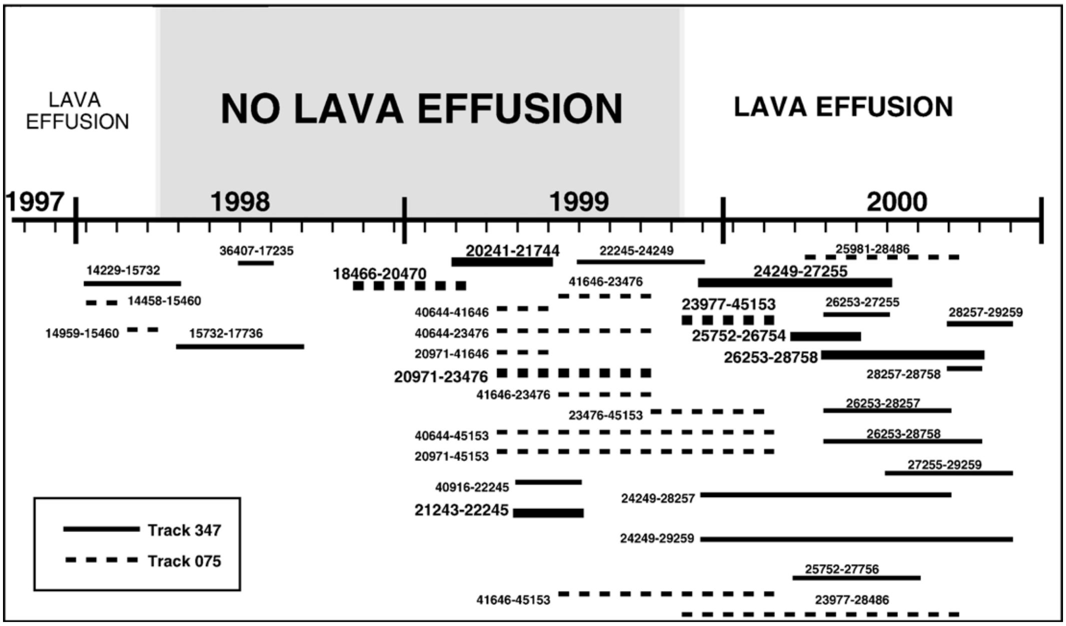


Fig. 2. Time lines of ERS radar interferograms (with perpendicular baselines less than 350 m) of Montserrat from 1998–2000, each tick below the line represents the 35 day interval between repeat orbits of ERS. The number pairs refer to the satellite orbits corresponding to the two radar images. Interferograms in bold are those used for far-field analysis. The period of no lava effusion at the volcano is shown schematically above.

Table 2
Meteorological data at time of selected ERS images of Montserrat

| Date[a] | ERS orbit | Wind[b] (m/s) | Rain[c] (mm/day) | ZWD[d] HERM 477 m | ZWD SOUF 448 m | ZWD SPRI 294 m | ZWD HARR 284 m | ZWD MVO1 283 m | ZWD WTYD 191 m |
|---|---|---|---|---|---|---|---|---|---|
| 1mar98 | 14959 | 7 (E) | – | 15 | 15 | 20 | 15 | **18** | 17 |
| 5apr98 | 15460 | 13 (E) | – | **57** | 55 | 75 | 57 | 68 | **65** |
| 24apr98 | 15732 | 2 (W) | – | **76** | 72 | 97 | 74 | **96** | **74** |
| 2jul98 | 36407 | 9 (W) | – | **107** | 102 | 137 | 105 | **130** | **112** |
| 7aug98 | 17235 | 1 (E) | – | **169** | 158 | 212 | **166** | **187** | **179** |
| 1nov98 | 18466 | 8 (ESE) | – | **140** | 132 | 178 | 136 | **156** | **157** |
| 5mar99 | 20241 | 10 (E) | 24 | **43** | 43 | 58 | 45 | **51** | **55** |
| 21mar99 | 20470 | 7 (ENE) | 0 | **56** | 56 | 76 | 58 | **77** | **61** |
| 8apr99 | 40415 | 11 (ENE) | 6 | **100** | 95 | 129 | **99** | **114** | **111** |
| 9apr99 | 20742 | 10 (E) | 5 | **155** | 155 | 191 | 150 | **175** | **166** |
| 24apr99 | 40644 | 10 (E) | 1 | **61** | 65 | 87 | 67 | **87** | 75 |
| 25apr99 | 20971 | 10 (E) | 0 | **102** | 106 | 143 | 110 | **127** | **137** |
| 13may99 | 40916 | 9 (SE) | 0 | **104** | 99 | 133 | 102 | **119** | **115** |
| 14may99 | 21243 | 11 (SE) | 0 | **100** | 98 | 132 | 101 | **120** | **115** |
| 18jun99 | 21744 | 7 (ENE) | 1 | **101** | **121** | **158** | **112** | 135 | **127** |
| 3jul99 | 41646 | 3 (NW) | 13 | 92 | **107** | **123** | **92** | **108** | 109 |
| 4jul99 | 21973 | 12 (NW) | 0 | **63** | **80** | **105** | **68** | **77** | **103** |
| 23jul99 | 22245 | 1 (SSE) | 13 | 124 | **103** | **168** | **127** | **154** | 139 |
| 17oct99 | 23476 | 10 (E) | 1 | 108 | 121 | 163 | 124 | **163** | **146** |
| 21nov99 | 23977 | 16 (NE) | 6 | 133 | 128 | 173 | 132 | **157** | 149 |
| 10dec99 | 24249 | 10 (ENE) | 0 | 72 | **82** | 93 | **50** | **85** | **90** |
| 4mar00 | 45153 | 11 (E) | 0 | **18** | 27 | 36 | **20** | **40** | **44** |
| 24mar00 | 25752 | 11 (E) | 11 | 9 | **4** | **12** | 9 | 11 | **16** |
| 9apr00 | 25981 | 9 (E) | 9 | 80 | 77 | 103 | **79** | **94** | **89** |
| 28apr00 | 26253 | 12 (E) | 12 | 36 | **35** | **45** | **16** | **37** | **68** |
| 2jun00 | 26754 | 1 (NNE) | 1 | **32** | **49** | **73** | **29** | **59** | **52** |
| 7jul00 | 27255 | 4 (NW) | 4 | **102** | 100 | **116** | **92** | **105** | **125** |
| 11aug00 | 27756 | 5 (N) | 5 | **98** | **105** | **136** | **86** | 122 | **133** |
| 15sep00 | 28257 | 3 (W) | 3 | **132** | 135 | **175** | **139** | **154** | **185** |
| 1oct00 | 28486 | 7 (E) | 7 | **167** | 180 | **191** | **160** | **253** | **204** |
| 20oct00 | 28758 | 5 (E) | 5 | **175** | **190** | **194** | **173** | **189** | **207** |
| 24nov00 | 29259 | 5 (E) | 5 | **177** | **204** | **222** | **216** | **201** | 212 |

Bold values are measured, non-bold are average values.
[a] Time of each overpass is about 02:39 GMT, 22:39 local time on the previous day.
[b] Wind vectors from the ECMWF operational analysis model at height of about 1 km.
[c] Rainfall daily rates from Hope station, about 6 km northwest of the volcano.
[d] GPS ZWD values in millimetres at time of ERS overpass calculated using GIPSY software. Altitude of stations in metres is shown at top of columns.

times of radar imaging. This wide range is caused by the low altitude of the GPS sites and the often high humidity values in the tropics.

### 3.1. GPS water vapour estimation

The total atmosphere delay for GPS L-band signals can be partitioned into a dispersive, frequency dependent component, and non-dispersive, non-frequency dependent component (Spilker, 1980). The dispersive portion of the delay arises from the ionosphere and can be effectively removed by observing both L1 and L2 carrier phases using dual-frequency receivers. The majority of the path delay, however, arises from the neutral atmosphere, primarily the troposphere, which is non-dispersive and thus cannot be removed from the data directly by dual-frequency observations. GPS processing takes two approaches to removing the troposphere delay, which is further divided into “dry” or hydrostatic and “wet” components (Saastamoinen, 1972; Davis et al., 1985). Both components are strong functions of elevation angle and have minima at zenith above the site. One approach is to use a stochastic estimation of the apparent temporal behaviour of the wet troposphere at the same time as the inversion of geodetic parameters from the GPS data stream (Tralli and Lichten, 1990). The stochastic method is the one employed by GIPSY-OASISII and used here to derive the ZWD (Lichten, 1990). The version of GIPSY employed for this analysis makes no provision for vertical tropospheric gradients. At each epoch of observation, in this case the original 30 s observation data were decimated to 5 min, the ZWD is estimated along with the topocentric position of the receiver in order to yield the final, smoothed, globally-averaged, best-fit final solution for the station position. We assumed that the tropospheric drift was $1.7\times10^{-7}$ km/s and the a priori sigma was set to 0.5 m for ZWD estimation. The Niell tropospheric mapping function was employed in all calculations (Niell, 2000). Final earth orientation and precise orbit parameter files were obtained from NASA's Jet Propulsion Laboratory and a non-fiducial, precise point positioning strategy was adopted for the GPS analysis (Blewitt et al., 1992; Heflin et al., 1992). These techniques are similar to those employed by Mattioli et al. (1998).

### 3.2. InSAR correction

Generally, water vapour contents in the troposphere decrease upward. So in an idealised, horizontally stratified troposphere any topographic relief would modulate the total water vapour delay by simple intersection with this trend (e.g., Delacourt et al., 1998). However, air masses advecting around mountains and involved in convective cells produce local horizontal gradients (e.g., Hauser, 1989; Wadge et al., 2002b). Advection of moist air over Soufrière Hills is often apparent from the cloud cap that forms. The Northeast Trades ensure that winds from the east and northeast dominate in Montserrat. However, Table 2 shows that the winds do vary in strength and direction and thus the pattern of advection of water vapour over the volcano varies through the year. Hence there is a need for both an absolute calibration of water vapour content and a measure of its spatial pattern. We have used the ZWD values to create a spatial mapping of water vapour delays on Montserrat that existed during SAR image collection. Table 2 also shows that daily rainfall rates do not correlate strongly with ambient ZWD values during the ERS satellite overpass. This is not surprising given the highly localised and short duration nature of much rainfall on the island. Rain droplets and cloud have much less of a delaying effect on C-band radar than water vapour, though very localised cumulus rain clouds can produce an additional delay of a few millimeters (Hanssen, 2001).

The GPS ZWD estimates are derived from path delays measured within a conical space with its apex at the receiver, and thus represent a sampling of tropospheric water vapour that becomes more diffuse upwards (Hanssen, 2001, Fig. A2). The average spacing of the GPS receivers on Montserrat is about 3.5 km (with an average altitude of about 300 m above sea level (asl)) and for a GPS satellite-viewing cut-off angle of 10°, receivers this far apart overlap above an altitude of about 600 m (Fig. 3a). Hence most of the difference between contemporaneous ZWD values on Montserrat must be due to the variable water vapour between sea level and 600 m altitude and any variability above this height will be highly smoothed. Because almost all the long-term coherent surface of the volcano (Fig. 1) is below about 700 m asl, then the individual ZWD values

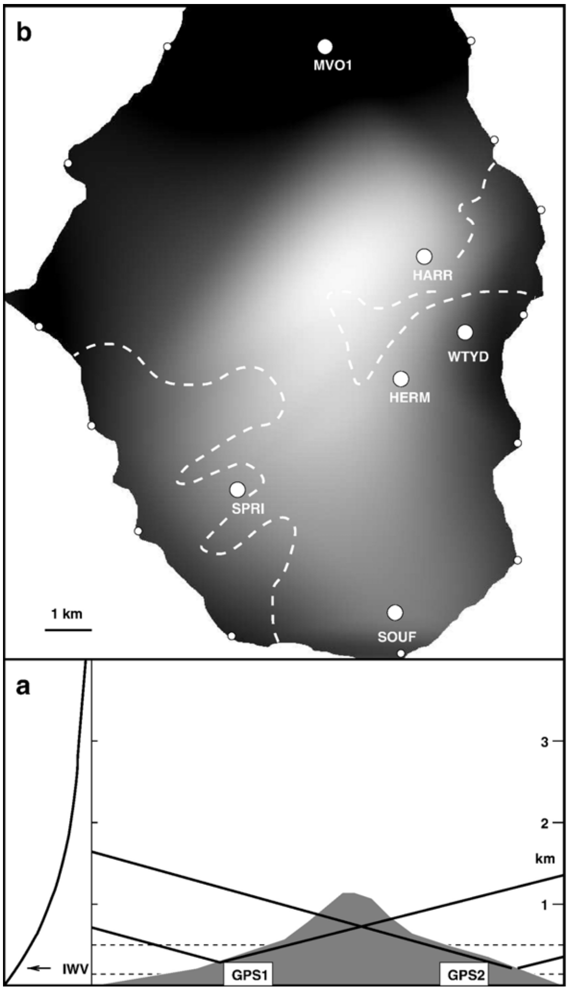


Fig. 3. (a) Cartoon section through the volcano and the lower troposphere. Two GPS receivers (GPS1, 2) with 10° cut-off angles are shown to indicate the regions sampled by the respective zenith wet delay estimates. Dashed lines show the altitudinal limits of the GPS sites on Montserrat. The schematic plot on the left shows a typical reduction of IWV with altitude. (b) Example interpolated ZWD field as a grey tone. Locations of the six continuous GPS receivers on Montserrat used in this study. Un-named circles are the locations of the sea-level ZWD values assumed from a linear extrapolation of the HERM-WTYD values. Approximate limits of the areas of long-term coherence are shown with a dashed line (see Fig. 1).

at the six sites should represent the local spatial variability over these parts of the volcano's surface reasonably well at length scales of a few kilometres. The six GPS sites range from 191 to 477 m above sea level and hence are not representative of the generally higher water vapour contents from 191 m to sea level, which is also the altitude range of many of the coherent surfaces (Fig. 1). To account for the water vapour below the GPS receivers, a linear gradient between ZWD values at the neighbouring HERM (477 m asl) and WTYD (191 m asl) GPS sites is extrapolated to a value at sea level and this value seeded at points on the coast (Fig. 3b). Although the general decrease of water vapour with altitude is exponential (Webley et al., 2002; Foster and Bevis, 2003), a linear extrapolation over this range introduces little error. A water vapour field is then interpolated between the six observed ZWD values and the sea-level points using a polynomial surface fit to a Delauney triangulation about the sites. Unfortunately, at the times of the ERS images ZWD estimates are not available for all sites. For missing data, values are calculated from the average of the other observed measurements at that time weighted by the long-term average value at that site (non-bold values in Table 2). Also we require the delays to be calculated along the slanted path of the radar which is at about 23° from the vertical, the Slant Wet Delay (SWD), and we applied an appropriate (1/cos 23°) factor prior to interpolation. The difference between two such delay fields at the time of the ERS overpasses gives the correction required to the differential interferograms. Fig. 4 shows an example of this applied to the unwrapped interferogram collected between 3 to 4 July 1999.

We can also improve our quality control over the water vapour effect by using simple statistical range and dispersion measures of the ZWD data. Table 3 summarises these, where available, for selected interferograms. Pairs with low absolute values of average delay across all sites should have generally low spatial variation of delays. Only two pairs have average ZWD values less than 100 mm (Table 3) for each individual image. The differences between the average values of each pair indicate how similar the general humidity values of the island were at the times of radar overpass. Again, low difference values should mean smaller delay effects locally too. For example, pair 20971-23476 has individual ZWD estimates that are quite high, but similar, giving a low difference (−16 mm). Site-specific differences in measured ZWD values will bring out the spatially variable character of the water vapour field. When the standard deviation of these (rather than the difference of the averages) is low, then the amplitude of the spatial anomalies in the delay field should also be low. Pair 26253-28758 has a very high difference between averaged ZWD values but the standard deviation of individual site differences is low. Finally, in Table 3 we report the range in SWD values of the interpolated correction fields over the coherent areas of the interferogram and the equivalent interferogram ranges. A small correction range relative to the interferogram should generally mean a higher quality interferogram. The bold values in Table 3 are those that satisfy criteria,

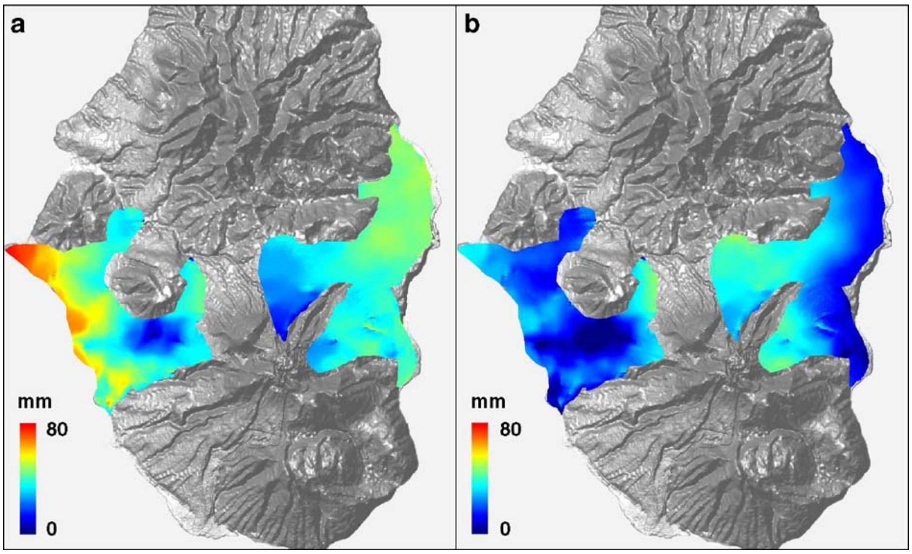


Fig. 4. (a) Unwrapped differential interferogram for the 1 day between 3 and 4 July 1999 (41646-21973), showing an apparent line-of-sight movement of the upper, parts of Soufriere Hills volcano away from the satellite (downwards) relative to the lower flanks during this period and, (b) same interferogram after correction by the GPS-derived water vapour image.

Table 3
Atmospheric selection criteria for interferograms

| InSAR pair | Interval (days) | Average ZWDs (mm)[a] | Difference average ZWD (mm)[b] | Individual site ZWD differences (mm)[c] | (s.d.) | Correction field range (mm)[d] | InSAR range (mm)[e] | Select |
|---|---|---|---|---|---|---|---|---|
| 14959-15460 | 35 | **17–64** | **−47** | | | **20** | **60** | yes |
| 36407-17235 | 36 | 116–179 | −63 | −62 −57 −67 | **(5)** | **17** | **56** | yes |
| ***18466-20470*** | 140 | 151–60 | 91 | 84 79 96 | **(9)** | 29 | **56** | yes |
| ***20241-21744*** | 105 | 49–126 | −77 | −58 −72 | **(10)** | **38** | **78** | yes |
| 40916-22245 | 71 | 120–134 | **−14** | −35 | | 46 | 42 | no |
| ***21243-22245*** | 70 | 111–134 | **−23** | −34 | | **19** | **56** | yes |
| 22245-24249 | 140 | 134–79 | 55 | 69 77 21 | (30) | **26** | **56** | yes |
| 40644-23476 | 176 | 71–138 | −67 | −76 | | 63 | 56 | no |
| ***20971-23476*** | 175 | 122–138 | **−16** | −36 −9 | **(19)** | **11** | **84** | yes |
| 41646-23476 | 106 | 105–138 | **−33** | −55 | | 31 | **56** | yes |
| 21973-23476 | 105 | 83–138 | −55 | −86 −43 | (30) | **24** | **56** | yes |
| 23977-28486 | 315 | 143–192 | **−49** | −96 | | 66 | 56 | no |
| ***23977-45153*** | 104 | 143–31 | 112 | 117 | | 43 | **56** | yes |
| 25981-28486 | 175 | 87–192 | −105 | −81 | | 53 | **56** | no |
| ***24249-27255*** | 210 | 79–107 | **−28** | −20 −35 −42 | **(11)** | 19 | **42** | yes |
| ***25752-26754*** | 70 | **9–49** | **−40** | −36 −61 −45 | **(10)** | 42 | **56** | yes |
| 27255-29259 | 140 | 107–206 | −99 | −75 −96 −124 −106 | **(19)** | 33 | **40** | yes |
| 24249-28257 | 280 | 79–155 | −76 | −69 −95 −89 | **(14)** | **52** | **112** | yes |
| 24249-29259 | 350 | 79–206 | −127 | −116 −166 −122 | (27) | 49 | **84** | yes |
| 25752-27756 | 140 | 9–109 | −100 | −117 −124 −101 | **(12)** | 58 | 42 | no |
| 26253-27255 | 70 | 43–107 | −64 | −68 −57 −76 −71 | **(7)** | 40 | **69** | yes |
| 26253-28257 | 140 | 43–155 | −112 | −117 −117 −123 −130 | **(5)** | 65 | 42 | no |
| ***26253-28758*** | 175 | 43–188 | −145 | −152 −139 −157 −149 −155 | **(7)** | **20** | **56** | yes |
| 28257-29259 | 70 | 155–206 | −51 | −45 −47 −77 −47 | **(14)** | 60 | 56 | no |

Values in bold satisfy the following criteria:
Bold InSAR pairs are those used in Figs. 7 and 8.
[a] Both average ZWD values < 100 mm.
[b] Difference in ZWD averages < 50 mm.
[c] Standard deviation < 20 mm.
[d] Correction range < 0.5 InSAR range.
[e] InSAR range > correction range.

albeit arbitrary, based on these measures. We reject seven of these interferograms that satisfy less than two of these criteria as being too likely to have significant residual atmospheric artefacts.

## 4. Ground motion

The ERS SAR in ascending passes views the surface along an azimuth just south of east and at an inclination of about 23° from vertical. Hence it records largely the vertical component of any surface motion. There are three, spatially and temporally distinct, types of vertical ground motion apparent in the Montserrat InSAR results: contraction of pyroclastic flow deposits, near-field motion and far-field motion.

### *4.1. Pyroclastic flow deposit contraction*

The valleys that radiate from the Soufrière Hills Volcano have been buried to varying degrees by pyroclastic flow deposits, in particular during the most productive 1997 period (Wadge et al., 2002a). The valleys of White River, Mosquito Ghaut, Tuitt's Ghaut and the Tar River had the thickest deposits, exceeding 100 m in places in early 1999 (Wadge, 2000). The emplacement temperatures of the block-and-ash flow deposits were sometimes greater than 400 °C (e.g., Cole et al., 2002). There are a few systematic measurements of temperature profiles for the uppermost two metres of deposits of large flows during 1997 (MVO records). These show that the rate of cooling at a depth of one metre below the surface during 1998 was about 0.19 °C/day between 198 and 271 days after emplacement of the deposit on 21 September 1997. This contrasts with a rate of about 2.6 °C/day for the first 38 days after emplacement at the same location. We would expect that this cooling would be accompanied by contraction and therefore that this rate of contraction would decrease with time.

ERS interferograms show clear evidence of subsidence in these buried valleys that are often only a few hundred metres across (Fig. 5). This is most obvious in

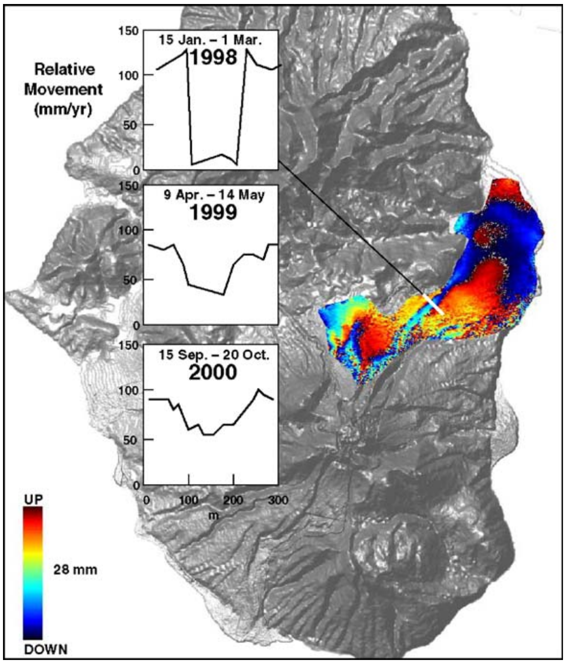


Fig. 5. An example of InSAR evidence for local subsidence of the surface above valleys buried by deep pyroclastic flow deposits. The image shows an interferogram for the northeastern slopes of Soufrière Hills for the 35 day period 15 January to 1 March 1998. Note that the interferogram is wrapped modulo 2 π, so that the colour cycle repeats every 28 mm of displacement, with the sense of motion of the surface relative to the satellite shown by the "up" and "down". The inset plot shows a profile of relative movement extracted from the interferogram across Tuitt's Ghaut (white bar in image). Equivalent profiles from interferograms one year (9 April–14 May 1999) and two years (15 September–20 October 2000) later show diminished rates of subsidence over this valley. The 1998 interferogram also shows more diffuse relative subsidence (blue areas) away from the valleys to the northeast where pyroclastic flow deposits had been emplaced a few months before.

those valleys where the deposits are thickest and the rates of subsidence are highest soon after emplacement. There is relatively little evidence of subsidence motion along the Fort Ghaut valley to the west (Fig. 1). Subsidence rates measured in Tuitt's Ghaut, where the deposits are about 50 m thick (Fig. 5), were about 150–120 mm/year in 1998, decreasing to 50–30 mm/year in 2000. This suggests that the subsidence is due to thermomechanical contraction, analogous to that measured on cooling, thick lava flows (Briole et al., 1997; Stevens et al., 2001) and is also reported from pyroclastic flow deposits at Augustine Volcano six years after emplacement (Lu et al., 2003). Interferometric coherence within some of these valleys tends to be lost over periods of greater than 70 days. This is probably mainly due to the occasional passage of mudflows after heavy rain (Matthews et al., 2002).

### 4.2. Near-field motion

Processes acting within the dome and the uppermost part of the feeder conduit, in the range 800–200 m below the dome surface (i.e., 200–800 m asl), appear to be able to transmit stresses to the surrounding rocks resulting in surface displacement out to a distance of about one kilometre, termed here near-field motion. This was recognised from surface EDM measurements (Jackson et al., 1998) and from tiltmeter measurements on Chances Peak, the old summit of the volcano (Voight et al., 1998) during 1995–97. Horizontal shortening to give finite, plastic strains were interpreted to be the combined result of intrusion, thermal expansion, surface loading by the dome and fracturing (Jackson et al., 1998; Shepherd et al., 1998), with the vertical component of motion being much smaller than the horizontal. The tiltmeters recorded cyclic, elastic strains of 5–20 microradians with periods of 6–14 h that were interpreted as pressurisation of the magma column in the uppermost conduit, particularly during the period of high flux, explosive behaviour of late 1997 (Voight et al., 1998).

ERS InSAR with its 35-day repeat cycle cannot capture short-period elastic strain cycles. Also, the area on and immediately around the dome is usually incoherent. However there are some interferograms that seem to show the effects of near-field motion. The more distal talus deposits from the dome in the Tar River valley typically show a subsidence signal, which may be a loading effect or deposit contraction. Less ambiguous are examples of local uplift in the near-field. Fig. 6 shows an uplift of about 40 mm over a period of 70 days

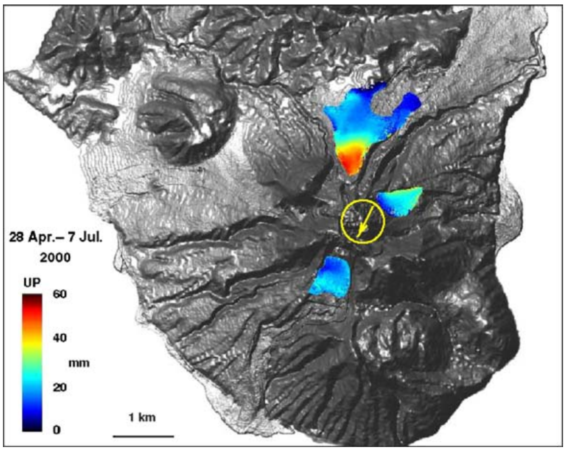


Fig. 6. Unwrapped differential interferogram of the upper part of Soufrière Hills Volcano for 28 April to 7 July 2000 (26253–27255) showing localised uplift of the area north of the dome (yellow circle). The arrow indicates the change of the locus of dome growth that occurred between 10–17 July 2000.

between 28 April and 7 July 2000 in the region to the north of the dome. This pattern is not seen in the Tar River valley to the east, nor in the Galways area to the south, where the signal is down towards the dome by about 20 mm. This period of measurement just precedes one of the periodic shifts in the locus of dome growth from the northeast to the southwest sector that occurred between 10–17 July 2000. The localised motion north of the dome is not seen in the preceding 70-day interferogram (Fig. 8c), suggesting that it occurred between 2 June and 7 July 2000. Another localised uplift of 20–30 mm in the same region is apparent in the interferogram that spans the period of 4 July to 17 October 1999, just prior to the resumption of lava effusion (not shown).

### 4.3. Far-field motion

We have seen that the areas near the dome (<1 km) and along the deeply-buried valleys are susceptible to motion signals unrelated to any deep magmatic crustal process. Thus we must look at those coherent surfaces outside of these areas, at distances from about one to six kilometres from the dome, in order to measure far-field motion due to strains associated with the magma reservoir system.

The thermal noise limit of measurement of phase using the ERS SARs is equivalent to about 1 mm of relative motion (Hanssen, 2001). Imprecise knowledge of the topography for some of the selected interferograms of Montserrat also could introduce errors of up to 5–10 mm. We described earlier how to minimise the effects of water vapour-induced noise in the InSAR signal by use of ZWD-based selection criteria and corrections to the interferograms using models of the water vapour delay field (Table 3, Figs. 3, 4). Selected interferograms corrected in this way are considered as two groups with common secular deformation patterns: those from the period of no lava effusion (March 1998–

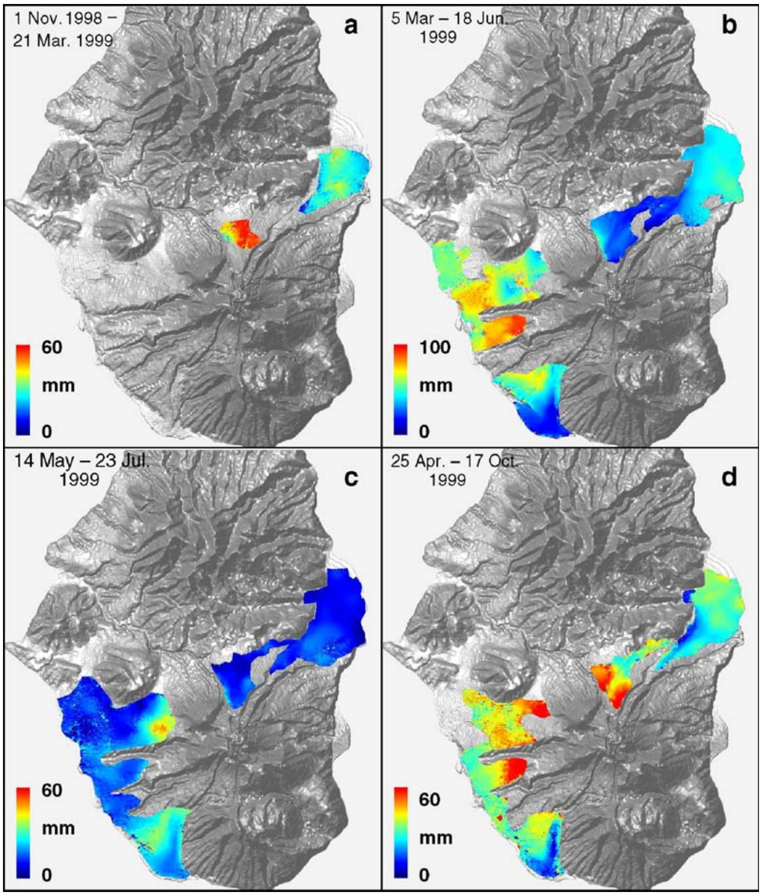


Fig. 7. Four selected images of line-of-sight displacement from the period of no lava effusion (Table 3) derived from InSAR measurements after correction for the atmospheric path delays in the following interferograms (parenthesised perpendicular baseline values in metres): (a) 18466-20470 (127), (b) 20241-21744 (192), (c) 21243-22245 (70), and (d) 20971-23476 (175). Blue to red represents line-of-sight shortening of the distance to the satellite (uplift) with time.

November 1999) and those from the period of lava effusion (December 1999–December 2000) shown as bold in Fig. 1 and those italicized in the first column of Table 3.

Fig. 7 shows four unwrapped and corrected interferograms with intervals of at least 70 days from the period of no lava effusion as maps of line-of-sight displacement. The differences in their areal coverage are a result of the different coherence levels over different periods. Interferograms b, c and d in Fig. 7 overlap in time during the second half of the period of no lava effusion from March to October 1999, and each shows a common pattern of uplift on the western slopes of the volcano. Because these three interferograms are derived from six independent SAR scenes and two orbital tracks, and if we assume a constant rate of displacement during this period, then we can average them in proportion to their duration. Such a "stacking" will suppress any residual, spatially-uncorrelated, atmospheric noise by a factor, in this case, of about 1.7 (square root of the number of interferograms) (Williams et al., 1998). The result of this is shown in Fig. 9. Areas with thick (>10 m) pyroclastic flow deposits (Wadge et al., 2002a) are outlined to show areas most susceptible to the effects of local subsidence of the deposits, which were about 50 mm/year or more in 1999. The stacked displacement field shows a relative gradient of up-to-the-summit motion on the lower western flanks by about 75–80 mm/year/km during the latter half of the quiescent period. It must be remembered that InSAR only provides relative motions, we do not know the motion in an absolute sense, or relative to a local datum such as sea level.

Four interferograms from the period of lava effusion (November 1999–December 2000) are shown in Fig. 8. Coherent areas are generally smaller than during the quiescent period, particularly on the northern and western slopes, but significant line-of-sight

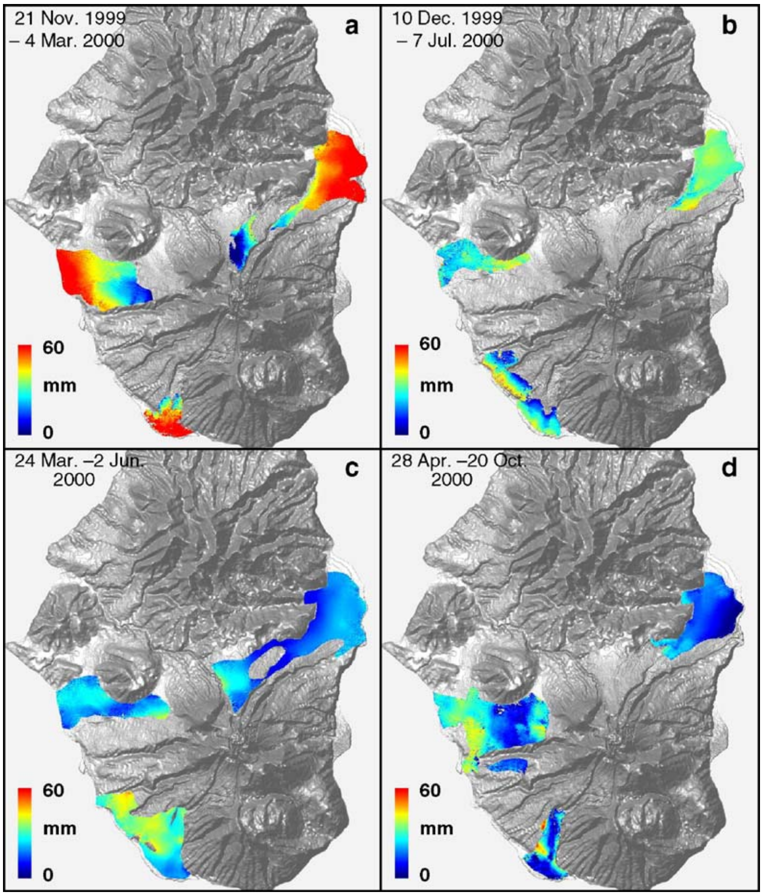


Fig. 8. Four selected images of line-of-sight displacement from the period of lava effusion (Table 3) derived from InSAR measurements after correction for the atmospheric path delays in the following interferograms (parenthesised perpendicular baseline values in metres): (a) 23977-45153 (231), (b) 24249-27255 (265), (c) 25752-26754 (146), and (d) 26253-28758 (126). Same colour scale applies to all four with blue to red representing shortening of the distance to the satellite (uplift) with time.

displacements are still seen. The interferograms do not show the same pattern of uplift that the interferograms of the latter half of the quiescent period do, rather they show gradients down towards the dome on the western side of the volcano. Fig. 9 shows the effect of stacking three of the interferograms (a, c, and d of Fig. 8) that represent the post-quiescence period. There is much less common overlap of areas of coherent signal on the western side of the volcano than for the stack from the quiescent period. The range of displacement rates is also about half that from the quiescent stack. On the northeastern slopes of the volcano, where long-term coherence is highest (Fig. 1) and away from the subsiding, valley-filling deposits, there is a down-to-the-summit gradient of relative motion of about 10–20 mm/year/km evident in the post-quiescence stack (Fig. 9).

There is therefore evidence from both the individual interferograms, and from their derived stacked products, to support far-field inflation of the volcano during the second half of the 1998–99 period of no lava effusion and deflation during the immediately succeeding period of renewed dome growth. The gradients of displacement are greater on the western side of the volcano than on the northeast (e.g., in the stacked result for the quiescent period (Fig. 9)). Possible reasons for this asymmetry will be discussed later.

## 5. GPS displacement measurements

The GPS network on Montserrat was designed to measure far-field 3D surface displacements. The horizontal velocities are measured within the Caribbean fixed frame of reference (DeMets et al., 2000) and the vertical velocities are relative to the Earth's centre of mass. Of the GPS sites only one, SPRI, falls within an area that is sometimes coherent in longer-period interferograms used to measure the far-field and even these measurements are not complete. Hence it is not possible to tie the InSAR relative motion displacements into the same reference frame of motion as the GPS measurements. In these circumstances joint inversion of the three-vector GPS data and the one-vector InSAR data within a source model of deformation is unlikely to be successful.

Nevertheless, a qualitative comparison of the two sets can be made. The vertical component of motion of the HARR site to the north of the volcano shows uplift of about 45 mm/year from 1998 through 1999 (Fig. 10). During this period, roughly corresponding to the period of no lava effusion, the horizontal components of displacement, for all sites, were away from the summit of the volcano in an approximately radial pattern. The horizontal motions on the western side of the volcano were generally greater those on the eastern side. This

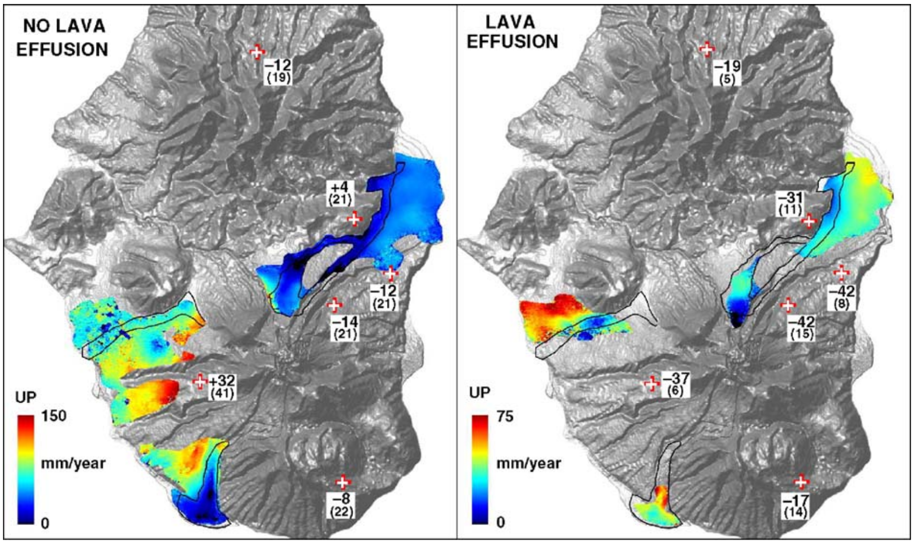


Fig. 9. Averaged images of InSAR-measured line-of-sight annual displacement rates for part of the period of no lava effusion (March 1999 to November 1999) and succeeding period of lava effusion (November 1999 to October 2000) resulting from stacking three corrected interferograms in each case (20241-21744, 21243-22245, 20971-23476 and 23977-45153, 25752-26754, 26253-28758, respectively). The black lines outline the areas with more than 10 m depth of pyroclastic flow deposits from 1997. Also shown are the equivalent radar line-of-sight motion rates (mm/yr, one sigma uncertainties in brackets) measured by the six CGPS sites (white and red crosses) for the same periods. Note that although the GPS rates are calculated relative to a fixed geodetic reference frame, the InSAR motion rates are solely differential, have no such reference frame and there is no direct correspondence between the absolute values of the two sets of measurements.

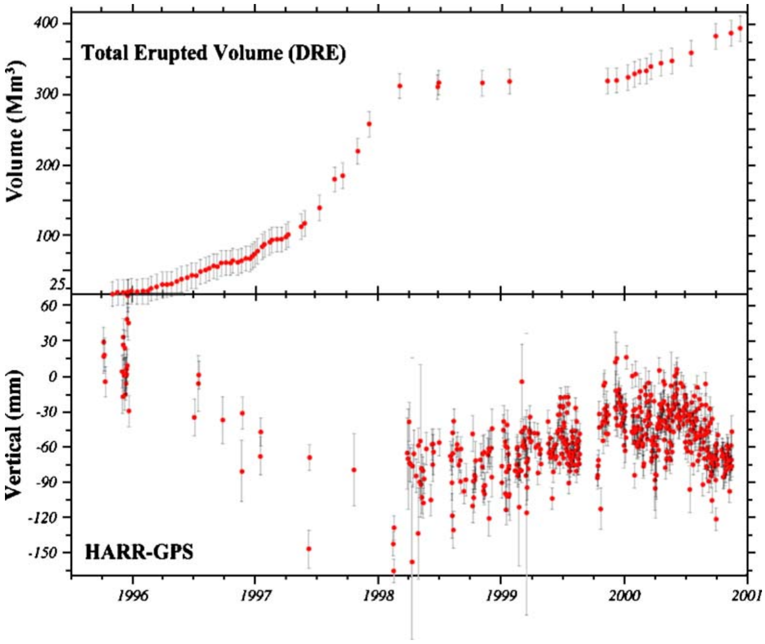


Fig. 10. Plots of vertical displacement of the HARR GPS receiver for 1995–2000 and the cumulative erupted volume for the same period (DRE = dense rock equivalent). Vertical position estimates (referenced to the Earth's centre of mass) were calculated using GOA-II v.2.6 with final JPL orbit, clock and earth orientation parameters using a 24 h absolute point position strategy. Formal errors (one sigma) are shown.

agrees broadly with the pattern of asymmetrical uplift seen from InSAR. For the shorter eight month period of no lava effusion represented in Fig. 9, the GPS-measured radar line-of-sight motion rates are noisy, but do seem to show relative uplift on the west (SPRI site). During the period of lava effusion in 2000 there is evidence of subsidence of the HARR site (Fig. 10) and all six other CGPS sites and the sense of horizontal motion of most of the GPS sites (HERM excepted) is directed toward the dome, consistent with a deep point source showing contraction and moderate opening across a NW-trending dike (Mattioli et al., 2000, 2002a,b). The GPS-measured radar line-of-sight motion rates for the period of lava effusion shown in Fig. 9 are much less noisy than those for the earlier period and show a pattern of increased rates of subsidence towards the dome. Additional details related to the GPS-derived deformation field will be reported elsewhere.

## 6. Hypotheses of crustal magma supply

The far-field deformation seen by both InSAR and GPS during the period of no lava effusion rules out an open magmatic system as defined in Table 1. The predicted observational differences between a depleting system with no deep re-supply and an unbalanced system with re-supply is that there is uplift strain when there is no lava effusion in the unbalanced system, but no equivalent strain for the depleting system. The InSAR (and GPS) observations favour an unbalanced magma supply system beneath Soufrière Hills Volcano.

Are the observed strains consistent with what is known about the magmatic system from other evidence? There is petrological evidence for storage of the andesitic magma at depths of about 5–6 km (Barclay et al., 1998), where some form of intimate heat exchange occurs between the andesite and basaltic magmas (Murphy et al., 1998). Devine et al. (2003) argue that most andesitic magma is transported to the surface within weeks of being re-heated by basaltic magma. The flux rate of magma erupted at the volcano increased to a rate over 7 $m^3\ s^{-1}$ at the end of the pre-quiescent period, giving an average of about 3.6 $m^3\ s^{-1}$ (Sparks et al., 1998). Since resumption of effusion in late 1999 the long-term flux rate has been more constant at about 2–3 $m^3\ s^{-1}$ (Herd et al., 2004) (Fig. 10).

Magma supply without effusion can occur in the unbalanced model. If we assume the reservoir at a depth of 6 km below sea level is supplied at a rate of 2 $m^3\ s^{-1}$ then we can calculate the surface displacements for a crust of known elastic properties. Fig. 11 shows such a crustal model based on a 2D axisymmetric finite element configuration, in which the reservoir is a sphere of 1 km radius embedded in a mid-crustal layer below an upper crustal layer with a base at −3 km

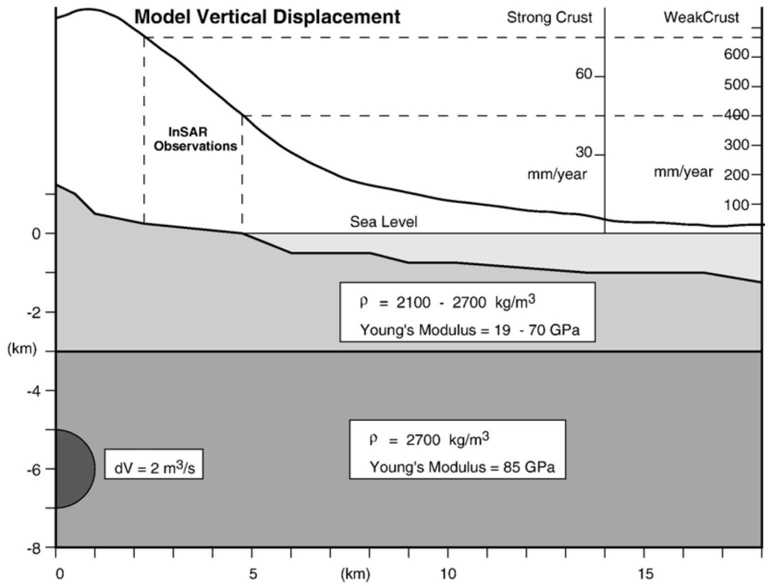


Fig. 11. Vertical displacement curve from a 2D axisymmetric finite element model of the surface displacement on Soufrière Hills Volcano due to a 1 km radius spherical magma chamber at 6 km depth filling at a rate of 2 $m^3$ $s^{-1}$. The dashed lines show the expected scale of displacement values corresponding to the region of InSAR measurements for two crustal models.

and an upper surface to the air and sea. The depth of the mid-upper crustal layer boundary is well constrained by regional seismic refraction data (Boynton et al., 1979). The scaling of the curve of surface vertical displacement due to such a model is sensitive to the local elastic properties of the crust, which are not well constrained beneath Montserrat. The zone 2 to 5 km from the volcano where most of the InSAR measurements are made corresponds to a nearly linear gradient in the vertical displacement curve. We present the model material properties in terms of density and Young's Modulus ($E$) to explore the extremes of behaviour for an island arc crust. The crustal model with a weak (compliant) upper layer (density = 2100 kg/$m^3$, $E$ = 19 GPa) has a surface displacement rate gradient of about 110 mm/year/km, compared to gradient values of about 12 mm/year/km for the crustal model with a strong (stiff) upper layer (density = 2700 kg/$m^3$, $E$ = 70 GPa). In reality, the bulk behaviour at the kilometre scale of this layer from −3 to +1 km asl will have a much smaller range and currently unknown spatial pattern. The InSAR stacked displacement rate (about 75–80 mm/year/km) for the period of no lava effusion falls between these values.

## 7. Discussion

The line-of-sight component of surface deformation of Soufrière Hills Volcano measured by InSAR during 1998–2000 is consistent with a model of magma supply in which magma entering a crustal magma chamber during the period of no lava effusion causes surface uplift. The pattern reverses during the resumption of magma effusion in 2000. The sense of these observations is the same as those measured by GPS. The spatial extent of the far-field motion InSAR data is too limited to attempt any meaningful inversion for source strength and location either alone or in conjunction with the GPS data. There also appears to be a discrepancy between the magnitude of the InSAR- and GPS-measured deformation rates and the asymmetry of the InSAR deformation relative to the putative pressure source beneath the vent/dome. Several factors could be responsible for this.

Firstly, the GPS coverage is poor on the western side of the volcano and so the InSAR signal there may represent an accurate measurement, not properly detected by the GPS observations. Secondly, the assumption of a constant strain rate during the two measurement epochs may be false. For example, short interval interferograms (e.g., 70 days) may give high rates of strain that are not sustained over a year and contribute an incorrectly-weighted annualised contribution to the stack.

Thirdly, there are a number of ways in which the water vapour delay may not have been correctly evaluated. Water vapour delay estimates from the continuous GPS receivers proved to be of great value in diminishing the effects of atmospheric water vapour noise on the surface displacements generally, both as a quality control measure and as a way of quantitative field removal. Better estimates could conceivably be made by seeking a tomographic inversion of the delays along individual paths, though a better altitudinal coverage of GPS receivers would be needed. The apparent disparity between the magnitudes of the inflation measured by InSAR and GPS could be explained by inaccuracies in the method of path delay correction. There is only one GPS site (SPRI) on the western slopes of the island. This station shows higher ZWD values than the other GPS stations at this altitude (HARR and MVO1) and sometimes higher values than station WTYD that is 100 m lower (Table 2). We note that the SPRI coordinate time series also is inconsistent with the other GPS sites and this may be related to the observed high ZWD. Local flow of moist air around the volcano could be responsible for a greater water vapour content around this site, and perhaps the western side of the island generally. If this were the case, then the interpolation scheme may not be representative of the true field. One contributory effect might be that because the sea-level values are extrapolated from the east coast, HERM-WTYD, pair of sites, they may be too low for the western side of the island (Fig. 3) and hence this would produce a path delay gradient that is too steep. Atmospheric flow modelling may help to understand this.

Another factor that could play a role is the plume of volatiles escaping from the dome. This plume is usually carried by the prevailing winds to the west. Most of the plume consists of water vapour, but only the accompanying sulphur dioxide flux is routinely measured and so we do not have any directly measured values of the magmagenic water vapour. The Soufrière Hills magma contains about 4–5 wt.% $H_2O$ in the rhyolitic melt phase at depth (Barclay et al., 1998) which comprises about 5–30% of the high-level magma flux (Sparks et al., 2000) at a rate of, say, 2 $m^3\ s^{-1}$. Taking the upper limits of these estimates gives 0.03 $m^3\ s^{-1}$ or 78 kg $s^{-1}$ (assuming a magma density of 2600 kg $m^{-3}$) of magmagenic water. This compares with estimates of 90–240 kg $s^{-1}$ for the water efflux rate based on the FTIR-measured $SO_2$:HCl ratio and UV spectrometer-measured $SO_2$ emission rates (Edmonds et al., 2002). If this is distributed along a horizontal length of 1 km (equivalent to the horizontal width of the plume) then the potential water loading rate per unit length is 0.078 kg $m^{-1}\ s^{-1}$. If we assume that all this water is in the vapour phase and not as cloud droplets, and that the water vapour is advected by a typical wind of 10 m $s^{-1}$ (Table 2), then the integrated vertical water vapour loading down the plume would be 0.0078 kg $m^{-2}$. This is equivalent to a radar delay of about 0.05 mm (Webley et al., 2002), which is negligible compared to the InSAR accuracy. The lava dome also generates water vapour by evaporating rainfall. Exceptionally, rainfall rates of 25 mm/hr are known on Montserrat (Matthews et al., 2002). To fix an upper limit, assuming complete evaporation over the whole area of the dome at this rainfall rate gives 5.5 $m^3\ s^{-1}$ of water, which is equivalent to about 35 mm of delay. This could potentially have a significant effect on the InSAR results. We do not have hourly rainfall data for the period of our measurements (Table 2), but it is unlikely that any of the radar data discussed here were collected in periods of very high rainfall rate as above. Also it is generally unlikely that all the precipitated water would be evaporated as assumed. So we might expect some local noise from this source, again on the downwind side of the volcano (usually the west), but perhaps at the level of a few millimetres.

Finally, there is the possibility of path delay effects caused by explosive events. Houlié et al. (2005) argue that delay transients of up to 290 mm, measured by GPS during explosions, are caused by high thermal gradients in explosive columns. For our case this is not a factor for the main interferograms analysed (Table 3), except perhaps that involving SAR acquisition 20971 on 25 April 1999.

## 8. Conclusions

1. InSAR and GPS measurements of surface deformation at Soufrière Hills Volcano, Montserrat are consistent with an unbalanced model of magma supply and crustal storage. In this model, observed inflation during the 1998–99 period of no lava extrusion and deflation during 2000, when lava flow resumed, are produced by magma reservoir pressurisation as new magma enters the reservoir and de-pressurisation as surface effusion exceeds supply.
2. Three types of surface motion can be distinguished in the InSAR measurements on Soufrière Hills Volcano: contraction of the thick pyroclastic flow deposits within valleys, localised deformation around the lava dome caused by shallow processes, and far-field deformation due to magma reservoir pressure changes in the crust.
3. C-band InSAR measurements on a volcano like Soufrière Hills Volcano are constrained by the small area of non-vegetated surfaces with coherent signals, the short window of temporal coherence (~one year) and the high levels of noise due to water vapour variability.

4. The effects of water vapour variability at Soufrière Hills Volcano can be corrected by using the Zenith Wet Delay estimates available from the six continuous GPS stations for the times of the radar overpasses. There is some evidence that the western side of the volcano, which has poor GPS coverage during this period, has the highest water vapour gradients. This may be an effect of predominant airflow patterns, or volcanic transients such as evaporation from the hot dome during heavy rainfall, but the background magmagenic water vapour input to the plume cannot be responsible. This highlights the potential value of good ambient meteorological measurements when performing InSAR in settings such as Montserrat.

## Acknowledgements

Bernd Scheuchl, Nicki Stevens and Charles Williams helped in the preparatory stages of this work, Kevin Hodges supplied the wind vector data and Adrian Matthews the rainfall data. We thank B. Darroux, A. Lopez, A. Matias and L. Rodriguez for their help during the re-installation of the continuous GPS network in early 1998. Support from ESA via an ERS data grant, from BNSC via the MONSAR project and from NERC via grant F60/G6/12/02 are gratefully acknowledged. ERS SAR data are copyrighted by the European Space Agency. The manuscript was improved by comments from two anonymous referees. GSM gratefully acknowledges support by the NASA Tropical Center for Space Sciences at the University of Puerto Rico at Mayagüez, NASA (award SENH NAG5-6031), NSF (award EAR 0116485) and the University of Arkansas.

## References

Amelung, F., Jonsson, S., Zebker, H., Segall, P., 2000. Widespread uplift and "trapdoor" faulting on Galapagos volcanoes observed with radar interferometry. Nature 407, 993–996.

Barclay, J., Carrol, M.R., Rutherford, M.J., Murphy, M.D., Devine, J.D., Gardner, J., Sparks, R.S.J., 1998. Experimental phase equilibria: constraints on pre-eruptive storage conditions of the Soufriere Hills magma. Geophy. Res. Lett. 25, 3437–3440.

Bevis, M., Businger, S., Herring, T.A., Rocken, C., Anthes, R.A., Ware, R.H., 1992. GPS meteorology: remote sensing of atmospheric water vapour using the Global Positioning System. J. Geophys. Res. 97, 15797–15801.

Blewitt, G., Heflin, M.B., Webb, F.H., Lindqwister, U.J., Malla, R.P., 1992. Global coordinates with centimeter accuracy in the International Terrestrial Reference Frame using GPS. Geophys. Res. Lett. 19, 853–856.

Boynton, C.H., Westbrook, G.K., Bott, M.H.P., Long, R.E., 1979. A seismic refraction investigation of the crustal structure beneath the Lesser Antilles island arc. Geophys. J. R. Astron. Soc. 58, 371–393.

Briole, P., Massonnet, D., Delacourt, C., 1997. Post-eruptive deformation associated with the 1986–87 and 1989 lava flows of Etna detected by radar interferometry. Geophys. Res. Lett. 24, 37–40.

Cabey, L., Wadge, G., 2001. Permanent scatterers on Montserrat. Proc. First Annual Conference Remote Sensing and Photogrammetry Society, 12–14 Sept., 2001, pp. 602–608.

Cole, P.D., Calder, E.S., Sparks, R.S.J., Clarke, A.B., Druitt, T.H., Young, S.R., Herd, R.A., Harford, C.L., Norton, G.E., 2002. Deposits from dome-collapse and fountain-collapse pyroclastic flows at Soufriere Hills Volcano, Montserrat. The Eruption of Soufrière Hills Volcano, from 1995 to 1999, Geological Society of London, Memoirs, vol. 21, pp. 231–262.

Davis, J.L., Herring, T.A., Shapiro, I.I., Rogers, A.E.E., Elgered, G., 1985. Geodesy by radio interferometry: effects of atmospheric modeling errors on the estimates of baseline length. Radio Sci. 20, 1593–1607.

Delacourt, C., Briole, P., Achache, J., 1998. Tropospheric corrections of SAR interferograms with strong topography. Application to Etna. Geophys. Res. Lett. 25, 2849–2852.

DeMets, C., Jansma, P.E., Mattioli, G.S., Dixon, T.H., Farina, F., Bilham, R., Calais, E., Mann, P., 2000. GPS geodetic constraints on Caribbean–North American plate motion. Geophys. Res. Lett. 27, 437–440.

Devine, J.D., Rutherford, M.J., Norton, G.E., Young, S.R., 2003. Magma storage region processes inferred from geochemistry of Fe–Ti oxides in andesitic magma, Soufrière Hills Volcano, Montserrat, W.I. J. Petrol. 44, 1375–1400.

Druitt, T.H., Kokelaar, B.P. (Eds.), 2002. The Eruption of Soufrière Hills Volcano, Montserrat, from 1995 to 1999, Geological Society of London, Memoir, vol. 21, pp. 664.

Dvorak, J.J., Dzurisin, D., 1997. Volcano geodesy: the search for magma reservoirs and the formation of eruptive vents. Rev. Geophys. 35, 343–384.

Edmonds, M., Pyle, D., Oppenheimer, C., 2002. HCl emissions at Soufriere Hills Volcano, Montserrat, West Indies, during a second phase of dome building: November 1999 to October 2000. Bull. Volcanol. 64, 21–30.

Foster, J., Bevis, M., 2003. Lognormal distribution of precipitable water in Hawaii. Geochem. Geophys. Geosyst. 4. doi:10.1029/2002GC000478.

Ghiglia, D.C., Pritt, M.D., 1998. Two-Dimensional Phase Unwrapping. John Wiley and Sons Inc., New York. 493 pp.

Goldstein, R.M., Werner, C.L., 1998. Radar interferogram filtering for geophysical applications. Geophys. Res. Lett. 25, 4035–4038.

Hanssen, R.F., 2001. Radar Interferometry. Data Interpretation and Error Analysis. Kluwer Academic Publishers, Dordrecht. 308 pp.

Hauser, J.P., 1989. Effects of deviations from hydrostatic equilibrium on atmospheric corrections to satellite and lunar laser ranging measurements. J. Geophys. Res. 94, 10182–10186.

Heflin, M., Bertiger, W., Blewitt, G., Freedman, A., Hurst, K., Lichten, S., Lindqwister, U., Vigue, Y., Webb, F., Yunck, T., Zumberge, J., 1992. Global geodesy using GPS without fiducial sites. Geophys. Res. Lett. 19, 131–134.

Herd, R.A., Mattioli, G.S., Sparks, R.S.J., 2004. Magma flux and ground motions at Soufriere Hills Volcano, Montserrat (1995–2004). Abstr. IAVCEI Conference, Pucon, Chile, October 2004.

Houlié, N., Briole, P., Nercessian, A., Murakami, M., 2005. Sounding the plume of the 18 August 2000 eruption of Miyakejima Volcano (Japan) using GPS. Geophys. Res. Lett. 32, L05302.

Jackson, P., Shepherd, J.B., Robertson, R.E.A., Skerritt, G., 1998. Ground deformation studies at Soufriere Hills Volcano, Montserrat: I. Electronic distance meter studies. Geophys. Res. Lett. 25, 3409–3412.

Lichten, S.M., 1990. Estimation and filtering for high precision GPS applications. Man. Geodesy 15, 159–176.

Lu, Z., Wicks Jr., C., Dzurisin, D., Power, J., Thatcher, W., Masterlark, T., 2003. Interferometric synthetic aperture radar studies of Alaska volcanoes. Earth Obs. Mag. 12/3 (6 pp.).

Matthews, A.J., Barclay, J., Carn, S., Thompson, G., Alexander, J., Herd, R., Williams, C., 2002. Rainfall-induced volcanic activity on Montserrat. Geophys. Res. Lett. 29. doi:10.1029/2002GL014863.

Mattioli, G.S., Dixon, T.H., Farina, F., Howell, E.S., Jansma, P., Smith, A.L., 1998. GPS measurements of surface deformation around Soufriere Hills Volcano, Montserrat from October 1995 to July 1996. Geophys. Res. Lett. 25, 3417–3420.

Mattioli, G.S., Rodriguez, L., Smith, A.L., Jansma, P.E., Herd, R.A., 2000. Changes in magmatic flux recorded by campaign and continuous GPS geodesy of Soufriere Hills, Montserrat, BWI. Abs. Geosciences 2000. Geol. Soc. London, p. 153.

Mattioli, G., Herd, R., Aponte, M., Dixon, T., Jansma, P., Smith, A., 2002a. The dynamics of an ongoing andesitic eruption: what we have learned from surface deformation at Soufriere Hills Volcano, Montserrat, BWI. Eos Trans. AGU 83, 19. (Spring Meet. Suppl., T31A-06).

Mattioli, G.S., Herd, R., Jansma, P.E., 2002b. Modeling of surface deformation cycles at Soufriere Hills, Montserrat from October 1995 to December 2001. Eos Trans. AGU 83, 47 (Fall Meet. Suppl., T12A-1309).

Murphy, M.D., Sparks, R.S.J., Barclay, J., Carroll, M.R., Lejeune, A.-M., Brewer, T.S., Macdonald, R., Black, S., Young, S.R., 1998. Role of magma mixing in triggering the current eruption at the Soufrière Hills Volcano, Montserrat, West Indies. Geophys. Res. Lett. 25, 3433–3436.

Niell, A.E., 2000. Improved atmospheric mapping functions for VLBI and GPS. Earth Planets Space 52, 699–702.

Norton, G.E., Watts, R.B., Voight, B., Mattioli, G., Herd, R.A., Young, S.R., Aspinall, W.P., Bonadonna, C., Baptie, B., Edmonds, M., Harford, C.L., Jolly, A.D., Loughlin, S.C., Luckett, R., Sparks, R.S.J., 2002. Pyroclastic flow and explosive activity of the lava dome of Soufriere Hills Volcano, Montserrat, during a period of virtually no magma extrusion (March 1998 to November 1999). The Eruption of Soufrière Hills Volcano, from 1995 to 1999, Geological Society of London, Memoirs, vol. 21, pp. 467–481.

Pritchard, M.E., Simons, M., 2004. Surveying volcanic arcs with satellite radar interferometry: the Central Andes, Kamchatka and beyond. GSA Today 14 (8), 4–11.

Saastamoinen, J., 1972. Atmospheric correction for the troposphere and stratosphere in radio ranging of satellites. In: Henriksen, S.W., Mancini, A., Chovitz, B.H. (Eds.), The Use of Artificial Satellites for Geodesy, Geophys. Monogr. Ser., vol. 15. AGU, Washington, D.C., pp. 247–251.

Shepherd, J.B., Herd, R.A., Jackson, P., Watts, R., 1998. Ground deformation measurements at Soufriere Hills Volcano, Montserrat: II. Rapid static GPS measurements June 1996–June 1997. Geophys. Res. Lett. 25, 3413–3416.

Sparks, R.S.J., Young, S.R., Barclay, J., Calder, E.S., Cole, P., Darroux, B., Davies, M.A., Druitt, T.H., Harford, C., Herd, R., James, M., Lejeune, A.M., Loughlin, S., Norton, G., Skerrit, G., Stasiuk, M.V., Stevens, N.F., Toothill, J., Wadge, G., Watts, R., 1998. Magma production and growth of the lava dome of the Soufriere Hills Volcano, Montserrat, West Indies: November 1995 to December 1997. Geophys. Res. Lett. 25, 3421–3424.

Sparks, R.S.J., Murphy, M.D., Lejeune, A.M., Watts, R.B., Barclay, J., Young, S.R., 2000. Control on the emplacement of the andesite lava dome of the Soufriere Hills Volcano, Montserrat by degassing-induced crystallization. Terra Nova 12, 14–20.

Spilker, J.J., 1980. GPS signal structure and performance characteristics. In: Janiczek, P.M. (Ed.), Global Positioning System, Papers Published in Navigation, vol. 1. The Institute of Navigation, Washington, D.C., p. 29.

Stevens, N.F., Wadge, G., Williams, C.A., Morley, J.G., Muller, J.-P., Murray, J.B., Upton, M., 2001. Surface movements of emplaced lava flows measured by SAR interferometry. J. Geophys. Res. 106, 11293–11313.

Tralli, D.M., Lichten, S.M., 1990. Stochastic estimation of tropospheric path delays in Global Positioning System geodetic measurements. Bull. Geod. 64 (2), 127–159.

Voight, B., Hoblitt, R.P., Clarke, A.B., Lockhart, A.B., Miller, A.D., Lynch, L., McMahon, J., 1998. Remarkable cyclic ground deformation monitored in real-time on Montserrat, and its use in eruption forecasting. Geophys. Res. Lett. 25, 3405–3408.

Wadge, G., 2000. A DEM of the volcanic deposits of Soufriere Hills Volcano during 1999. MVO Open File Report OFR 00-07.

Wadge, G., Scheuchl, B., Cabey, L., Palmer, M.D., Riley, C., Smith, A., Stevens, N.F., 1999. Operational use of InSAR for volcano observatories: experience from Montserrat. Proceedings FRINGE'99. ESA Publication SP478, Noorwijk, Netherlands.

Wadge, G., Cabey, L., Lomas-Clarke, S., Palmer, M.D., Smith, A., 2000. Operational use of InSAR for volcano observatories: experience in local reception at Montserrat. Proc. ERS-ENVISAT Symposium, 16–20 Oct. 2000, Gothenburg, Sweden.

Wadge, G., Scheuchl, B., Stevens, N.F., 2002a. Spaceborne radar measurements of the eruption of Soufriere Hills Volcano, Montserrat. The Eruption of Soufrière Hills Volcano, from 1995 to 1999, Geological Society of London, Memoirs vol. 21, pp. 583–594.

Wadge, G., Webley, P.W., James, I.N., Bingley, R., Dodson, A., Waugh, S., Veneboer, T., Puglisi, G., Mattia, M., Baker, D., Edwards, S.C., Edwards, S.J., Clarke, P.J., 2002b. Atmospheric models, GPS and InSAR measurements of the tropospheric water vapour field over Mount Etna. Geophys. Res. Lett. doi:10.1029/2002GL015159.

Webley, P.W., Bingley, R.M., Dodson, A.H., Wadge, G., Waugh, S.J., James, I.N., 2002. Atmospheric water vapour correction to InSAR surface motion measurements on mountains: results from a dense GPS network on Mount Etna. Phys. Chem. Earth 27, 363–370.

Williams, S., Bock, Y., Fang, P., 1998. Integrated satellite interferometry: tropospheric noise, GPS estimates and implications for interferometric synthetic aperture radar products. J. Geophys. Res. 103, 27051–27067.